Electronic Supplementary Material (ESI) for Journal of Materials Chemistry C.

Electronic Supplementary Information

Engineering large perpendicular magnetic anisotropy in amorphous ferrimagnetic gadolinium cobalt alloys

Karthik Srinivasan[1], Yulan Chen[2], Ludovico Cestarollo[2], Darrah K. Dare[3], John G. Wright[3], Amal El-Ghazaly[1]

[1]Department of Electrical and Computer Engineering, Cornell University, Ithaca, New York 14853, United States
[2]Department of Materials Science and Engineering, Cornell University, Ithaca, New York 14853, United States
[3]Cornell Center for Materials Research, Cornell University, Ithaca, New York 14853, United States

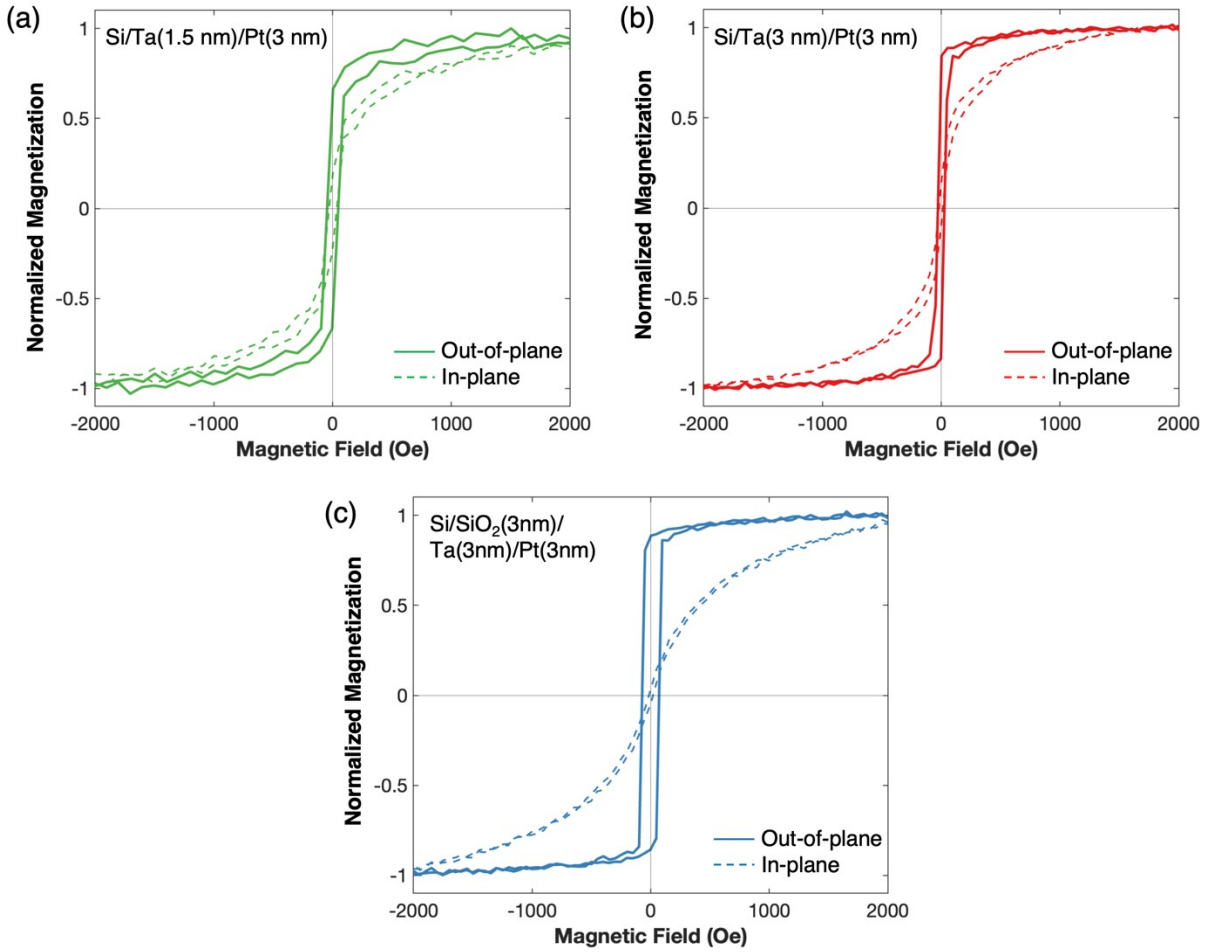

Figure S1. Out-of-plane and in-plane MH measurements of GdCo deposited on (a) Si/Ta(1.5 nm)/Pt(3 nm) [green], (b) Si/Ta(3 nm)/Pt(3 nm) [red] and (c) Si/SiO2(3nm)/Ta(3nm)/Pt(3nm) [blue]. Figures (a) and (b) indicate that the out-of-plane remanent magnetization improves with the Pt crystallinity (refer to Figure 1(a)). However, the inclusion of a 3 nm SiO_2, despite reducing the Pt polycrystallinity, still results in favorable PMA characteristics such as a large out-of-plane remanence ratio and an increase in the in-plane saturation field. While the reason for a favorable PMA with SiO2 (and reduced Pt crystallinity) is unclear and requires further studies, the MH loops show that a sensitive balance exists between the polycrystallinity of the underlying layers and the anisotropy of the Gd_xCo_{1-x}.

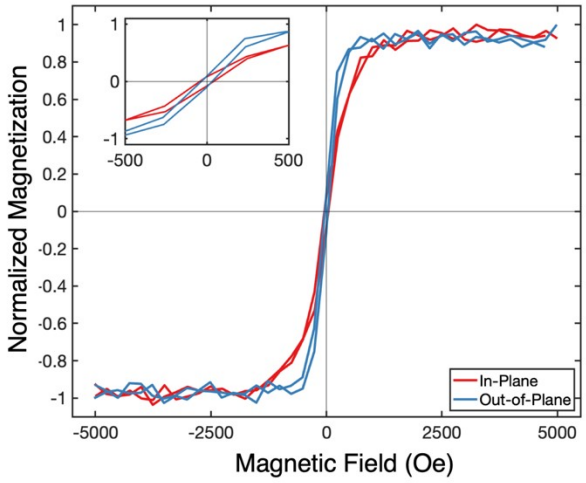

Figure S2. Magnetic hysteresis measurements of Gd_xCo_{1-x} samples sputtered on Si substrate with 6 nm of SiO_2 in a composite underlayer of $Si/SiO_2/Ta/Pt$. The inset shows that the remnant magnetization (M_R) for both the in-plane and out-of-plane measurements is less than 10% of the saturation magnetization (M_S).

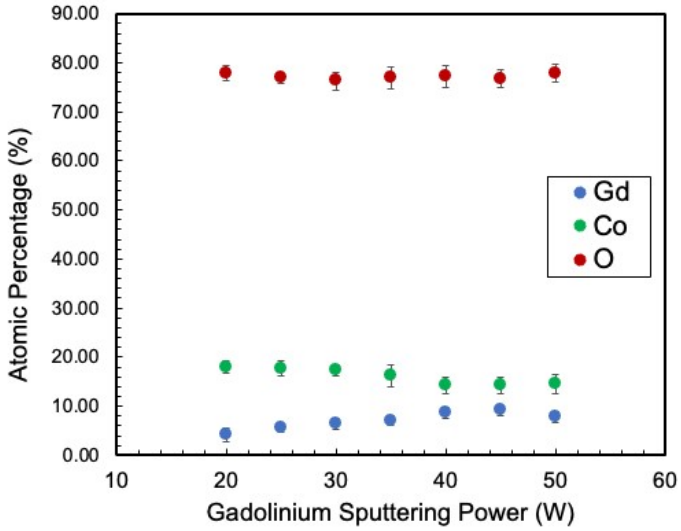

Figure S3. Atomic percentages of Gd, Co and O as obtained from energy dispersive x-ray spectroscopy (EDS). The EDS measurements are performed on samples that have a heterostructure of $Si/SiO_2/Ta/Pt/GdCoO/Pt$. As a result, the oxygen atomic percentage from GdCo is buried within the signal from the underlying SiO_2 layer, which is why the oxygen At% appears constant. Accurate oxygen content is obtained from XPS measurements.

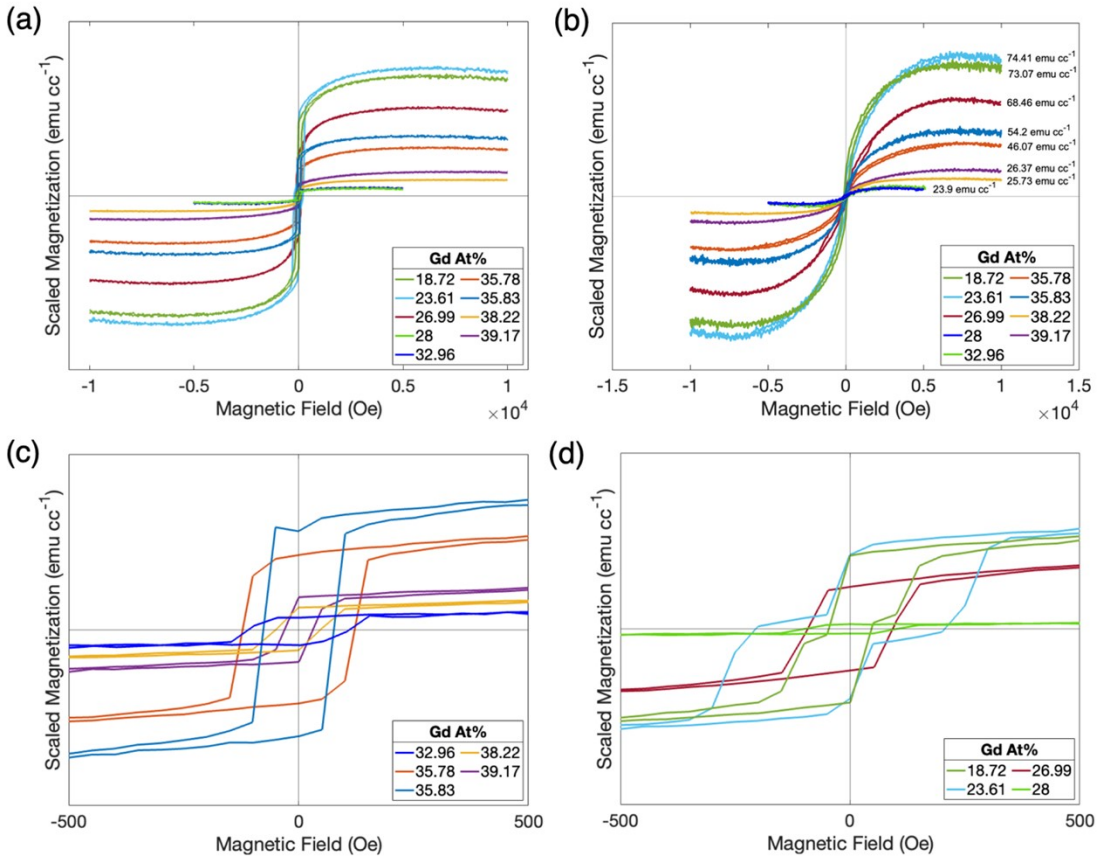

Figure S4. Magnetic hysteresis measurements of Gd_xCo_{1-x} samples sputtered with different Gd sputtering power that corresponds to varying Gd At% in the alloy. (a) Out-of-plane MH loops and (b) In-plane MH loops of Gd_xCo_{1-x} heterostructures show that saturation magnetization (shown in panel (b)) decreases up to Gd At% = 28 and increase beyond 32%. (c) Out-of-plane MH loops for Gd_xCo_{1-x} samples above the compensation window show square hysteresis behavior with different saturation magnetizations. (d) Out-of-plane MH loops for samples below compensation window show "bowtie" shaped hysteresis behavior indicative of magnetization reversal from two distinct sub-systems.

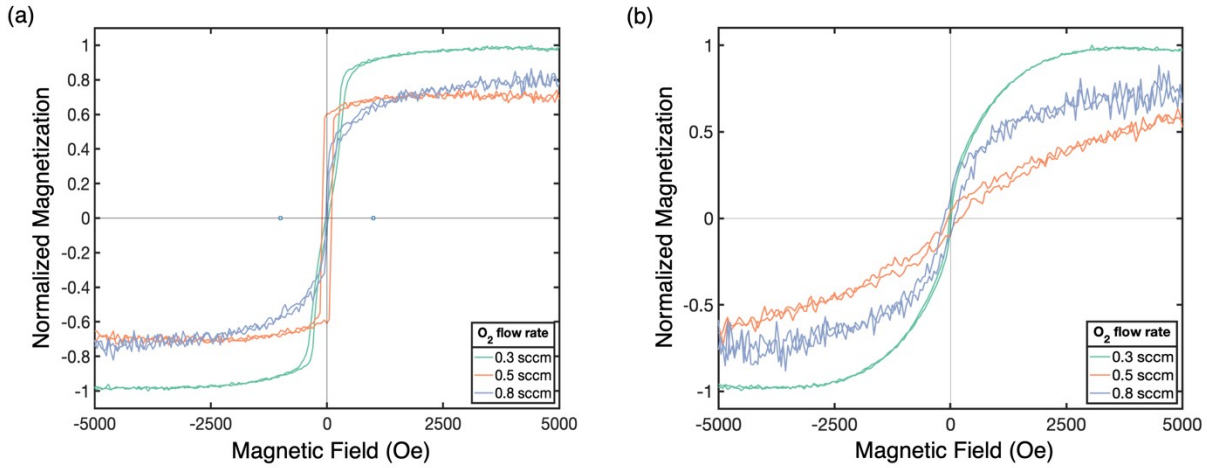

Figure S5. Magnetic hysteresis measurements of $Gd_xCo_yO_{1-x-y}$ for 0.3, 0.5 and 0.8 sccm of flow rate of oxygen. (a) Out-of-plane hysteresis measurements and (b) In-plane hysteresis measurements.

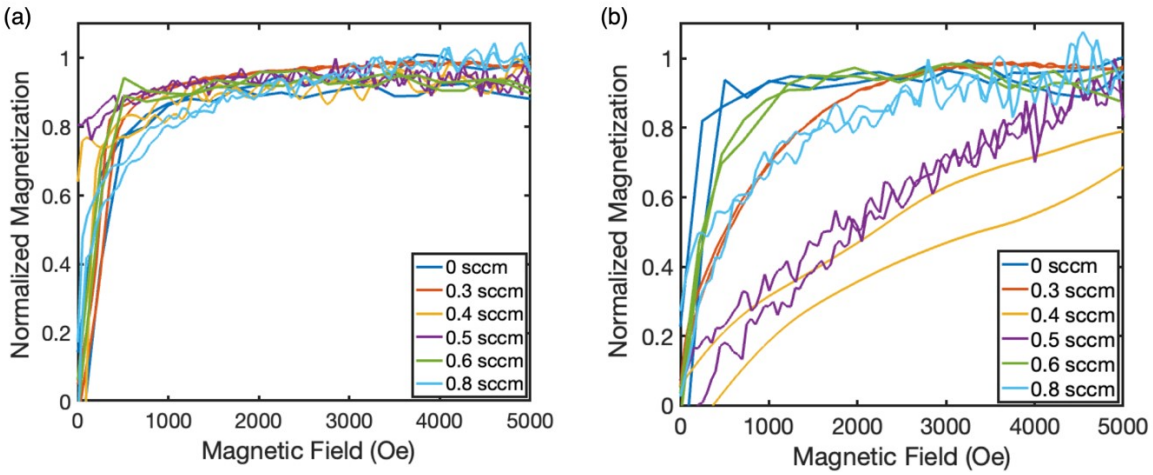

Figure S6. Magnetic hysteresis measurements of $Gd_xCo_yO_{1-x-y}$ for all oxygen flow rates between 0-0.8 sccm discussed in the paper. (a) Out-of-plane MH measurements. (b) In-plane MH measurements. Only the first quadrant of the MH loops is shown here for clarity.

Table S1. Summary of oxygen flow rates, in-plane saturation field and effective anisotropy energy density.

O_2 Flow Rate (sccm)	**$H_{saturation}$ - In-plane (Oe)**	**Effective Anisotropy Energy Density (erg cc^{-1})**
0	750	4.77E+03
0.3	2200	7.85E+04
0.4	4000	1.12E+05
0.5	4600	1.21E+05
0.6	1700	4.32E+04
0.8	1650	3.49E+04

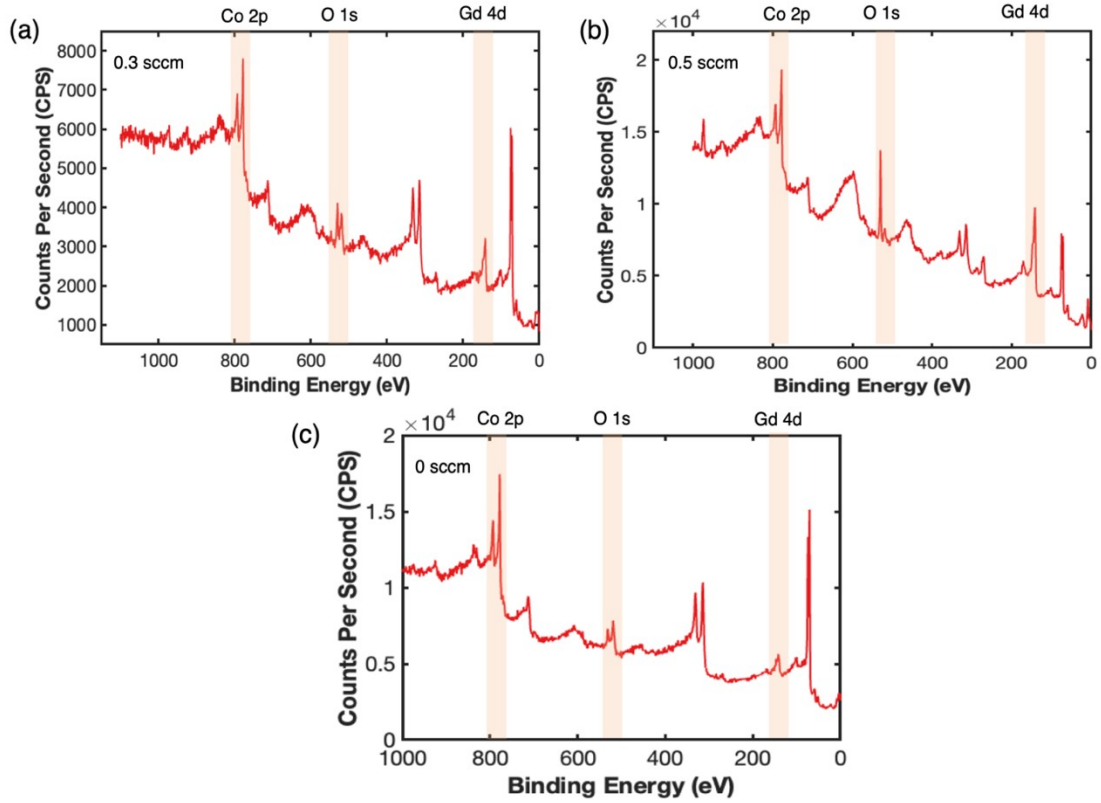

Figure S7. Full range XPS survey spectra for $Gd_xCo_yO_{1-x-y}$ alloy layers collected after 49 s of ion milling the heterostructure. (a) Samples sputtered with 0.3 sccm of reactive O_2. (b) Samples sputtered with 0.5 sccm of reactive O_2. (c) Samples sputtered without reactive O_2. The shaded regions represent the Co 2p, O 1s and Gd 4d peaks used in quantifying the role of oxygen in the alloys. XPS circumvents the issues faced in EDS characterization using TEM or SEM, as EDS falsely considers oxygen from the underlying SiO2 layer in the GdCo heterostructure. Through XPS, we are able to etch the top Pt layer and selectively characterize oxygen from the GdCo layer.

Table S2. Binding energies, areas under the fitted peak, computed atomic fraction and ratios of the area and atomic percentages for the hydroxide and oxide peak assignments for different O_2 flow rates.

O_2 Flow Rate (sccm)	**Assignment**	**Binding Energy (eV)**	**Area**	**Area Ratio**	**Atomic Percentage (%)**	**At% Ratio**
0	**OH^{-1}**	531.4	434.06	4.78	19.97	4.78
	Gd/Co Oxide	529.2	90.69		4.17	
0.3	**OH^{-1}**	531.6	376.07	1.18	19.31	1.18
	Gd/Co Oxide	529.4	318.94		16.38	
0.5	**OH^{-1}**	531.8	944.26	0.71	21	0.71
	Gd/Co Oxide	529.7	1320.09		29.35	

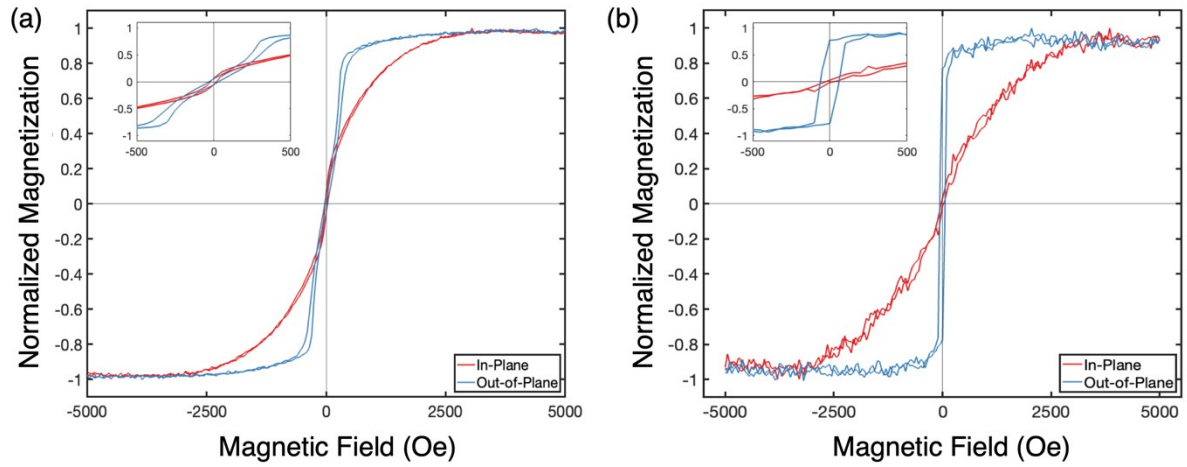

Figure S8. Role of reactive O_2 flow in $Gd_xCo_yO_{1-x-y}$ samples with sub-optimal flow rates. (a) MH loops from Gd_xCo_{1-x} heterostructures sputtered at 0.3 sccm of O_2 from pristine metallic targets show a non-square loop for the out-of-plane behavior, indicating that it is not the typical behavior expected of a sample with strong PMA. (b) MH loops from samples sputtered at 0.3 sccm of O_2 from targets that have been oxidized (or "seasoned") at 5 mTorr of O_2 for 60 seconds prior to reactive sputtering show the desired out-of-plane hysteresis. This implies that a specific cation to oxygen ratio is required to achieve the strong PMA.

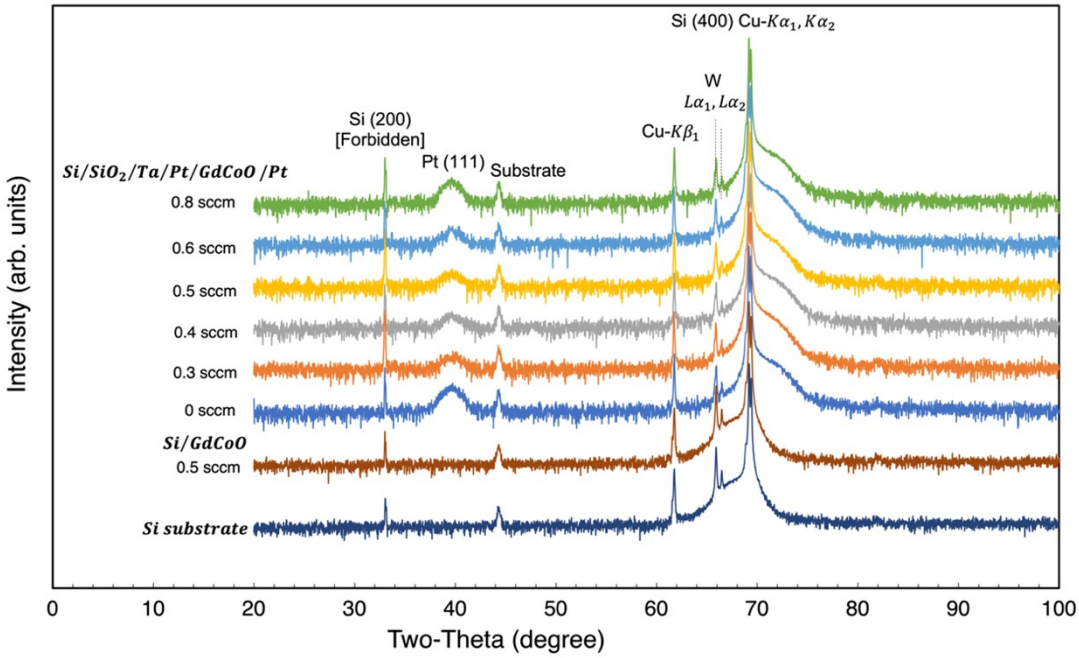

Figure S9. X-ray diffraction spectra of $Si/SiO_2/Ta/Pt/Gd_xCo_yO_{1-x-y}/Pt$ for different oxygen flow rates, Si/GdCoO and bare Si substrate. The Si/GdCoO sample sputtered at 0.5 sccm (which corresponds to a stoichiometry of $Gd_{21}Co_{28}O_{51}$) and the bare Si substrate, consists only peaks that correspond to the single crystal Si (100). The prominent Si(400) peaks at 69° and 69.3° correspond to the Cu Kα_1 ($\lambda = 1.5406$ Å) and Kα_2 ($\lambda = 1.5444$ Å) x-ray lines. The Si (200) peak at ~33° is forbidden but is seen due to a second-order (n=2) diffraction for Cu Kα_1. The peaks at ~62°, ~66° and ~66.5° correspond to the Si (100) from Cu Kβ_1 ($\lambda = 1.3922$ Å), W Lα_1 ($\lambda = 1.4764$ Å) and W Lα_2 ($\lambda = 1.4874$ Å) x-ray lines, which can be emitted from the X-ray source due to insufficient monochromation and collimation.